



## Hidden Symmetry-Broken Phase of MoS<sub>2</sub> Revealed as A Superior Photovoltaic Material

Journal:	<i>Journal of Materials Chemistry A</i>
Manuscript ID	TA-ART-06-2018-005459.R1
Article Type:	Paper
Date Submitted by the Author:	16-Jul-2018
Complete List of Authors:	<p>Xu, Meiling; Jilin University, State Key Lab of Superhard Materials            Chen, Yue; Department of Mechanical Engineering, The University of Hong Kong,            Xiong, Fen; The University of Hong Kong            Wang, Jianyun; Jilin University            Liu, Yanhui; Yanbian University, physics            Lv, Jian; Beijing computational science research center,            Li, Yinwei; Jiangsu Normal University, School of Physics and Electronic Engineering            Wang, Yanchao; Jilin University, State Key Laboratory of Superhard Materials            Chen, Zhongfang; University of Puerto Rico, Department of Chemistry            Ma, Yanming; Jilin University</p>

## Hidden Symmetry-Broken Phase of MoS<sub>2</sub> Revealed as A Superior Photovoltaic Material

Meiling Xu<sup>†,§</sup>, Yue Chen<sup>\*,‡</sup>, Fen Xiong<sup>‡</sup>, Jianyun Wang<sup>†</sup>, Yanhui Liu<sup>§</sup>, Jian Lv<sup>†</sup>, Yinwei Li<sup>§</sup>, Yanchao Wang<sup>\*,†,‡</sup>, Zhongfang Chen<sup>&</sup>, and Yanming Ma<sup>\*,†,#</sup>

<sup>†</sup>State Key Lab of Superhard Materials, College of Physics, Jilin University, Changchun 130012, China

<sup>§</sup>School of Physics and Electronic Engineering, Jiangsu Normal University, Xuzhou 221116, China

<sup>‡</sup>Department of Mechanical Engineering, The University of Hong Kong, Pokfulam Road, Hong Kong SAR

<sup>§</sup>Department of Physics, College of Science, Yanbian University, Yanji 133002, China

<sup>&</sup>Department of Chemistry, University of Puerto Rico, Rio Piedras Campus, San Juan, PR 00931, USA

<sup>#</sup>International Center of Future Science, Jilin University, Changchun 130012, China

### Corresponding Authors:

\* E-mail: [yuechen@hku.hk](mailto:yuechen@hku.hk)

\* E-mail: [wyc@calypso.cn](mailto:wyc@calypso.cn)

\* E-mail: [mym@calypso.cn](mailto:mym@calypso.cn)

## Abstract

Monolayer MoS<sub>2</sub> has long been considered as the most promising candidate for wearable photovoltaic devices. However, its photovoltaic efficiency is restricted by its large band gap (2.0 eV). Though the band gap can be reduced by increasing number of layers, the indirect band gap nature of the resulting multilayer MoS<sub>2</sub> is unfavorable. Herein, we report a theoretical discovery of the hitherto unknown symmetry-broken phase (denoted as 1T<sub>d</sub>) of monolayer MoS<sub>2</sub> through a swarm structure search. The 1T<sub>d</sub> phase has a distorted octahedral coordinated pattern of Mo, and its direct band gap of 1.27 eV approaches the optimal value of 1.34 eV that gives Shockley-Queisser limit for photovoltaic efficiency. Importantly, the direct band gap nature persists in thin films with multilayers owing to extremely weak vdW forces between adjacent 1T<sub>d</sub> layers. The theoretical photovoltaic efficiency at 30 nm thickness reaches ~33.3%, which is the highest conversion efficiency among all the thin-film solar cell absorbers known thus far. Furthermore, several feasible strategies including appropriate electron injection and proper annealing methods were proposed to synthesize the 1T<sub>d</sub> phase. Once synthesized, the superior photovoltaic property of the 1T<sub>d</sub> phase may lead to the development of an entirely new line of research for transition metal dichalcogenides solar cells.

Keywords: nanomaterials, MoS<sub>2</sub>, energy harvesting, photovoltaics

## Introduction

The efficient use of solar energy, one of the most important forms of renewable energy, provides a potential solution to solve the energy and environmental challenges facing the world. Various solar energy devices have been developed in the past decade, such as silicon-based, dye-sensitized, and perovskite solar cells. However, these devices often have bulky structures. Unique optoelectronic properties and chemical robustness of layered structures, two-dimensional (2D) transition metal dichalcogenides (TMDs) have many applications in optoelectronics<sup>1-3</sup>, catalysis<sup>4-9</sup>, spintronics, and valleytronics<sup>10,11</sup>. Especial for MoS<sub>2</sub>, it provides us new opportunities to develop portable, flexible, and wearable solar cells<sup>12</sup> as 2D solar cell material due to its high absorption coefficient ( $10^7 \text{ m}^{-1}$ )<sup>13-16</sup>.

Monolayer MoS<sub>2</sub> has three experimentally known polymorphs characterized by different coordination modes between Mo and S atoms, namely 1H, 1T and 1T'.<sup>17</sup> The 1H phase is most stable under normal conditions and is semiconducting, in which Mo adopts a trigonal prismatic coordination with S atoms. The 1T phase is characterized by the distorted layers and the octahedral coordination of Mo atoms, this metastable layer can be made via intercalation of 1H-MoS<sub>2</sub> lattice with alkali metals. The distortion of 1T phase with the formation of Mo-Mo metal bonds gives rise to the 1T' phase. Encouragingly, Zhang and coworkers just realized large-scale preparation of micrometre-sized metallic-phase 1T'-MoS<sub>2</sub>-layered bulk crystals in high purity.<sup>18</sup> 1T and 1T' phases are either metallic or large-gap quantum spin Hall insulator<sup>19</sup>, thus are hardly useful in terms of photovoltaic applications. Very recently, Du and coworkers theoretically predicted the not-yet-synthesized T'' phase of MoS<sub>2</sub>, which shows an intrinsic quantum spin Hall effect with a nontrivial gap and exhibits a topological phase transition driven by a small tensile strain.<sup>20</sup>

Monolayer MoS<sub>2</sub> in 1H phase (denoted as 1H-MoS<sub>2</sub>) with only ~0.65 nm shows a large absorption coefficient of  $10^7 \text{ m}^{-1}$  comparable to that of commercialized 50-nm-thick Si<sup>12</sup>, which makes it useful for wearable photovoltaic applications. However, the band gap (~2.0 eV) of monolayer 1H-MoS<sub>2</sub> is too large to give an ideal Shockley-Queisser absorption efficiency (33.7%) that requires an optimal band gap value of ~1.34 eV. As a result, monolayer 1H-MoS<sub>2</sub> can only absorb incident sunlight up to 5–10% in the visible wavelength region<sup>21</sup>. The fabrication demands and the physics of the absorption efficiency suggest that multilayer MoS<sub>2</sub> may be more attractive than single layer MoS<sub>2</sub> for photovoltaic applications since thin film has a much-reduced band gap. It has been reported that 300-nm film of MoS<sub>2</sub> can absorb up to 95% of the light<sup>22</sup>. Unfortunately, the major drawback of the MoS<sub>2</sub> thin film is the indirect nature of its band gap<sup>3</sup> where phonons are required to mediate electron excitations from light. Then, a question raises naturally: is there a new phase of MoS<sub>2</sub> monolayer with high experimental feasibility and a direct and smaller band gap in the range of 1-1.5 eV?

We here report a theoretical discovery of the hitherto unknown monolayer phase of MoS<sub>2</sub> (donated

as  $1T_d$ ) by carrying out the swarm-intelligence based CALYPSO structure searches. This  $1T_d$  monolayer is semiconducting with a direct band gap of 1.27 eV. More importantly, the direct band gap nature persists in the thin film due to the extremely weak vdW interactions in the multilayer structures of  $1T_d$  phase. The theoretical photovoltaic efficiency of  $1T_d$  phase reaches  $\sim 33.3\%$  at only 30 nm thickness, which is even higher than that of  $\sim 200$ -nm-thick GaAs ( $\sim 32.0\%$ ) and far beyond that of the conventional  $1H$  phase ( $19.0\%$ ). Our results also demonstrate that  $1T_d$  phase could be synthesized by a proper electron injection method. Once synthesized, the superior photovoltaic property of  $1T_d$ - $\text{MoS}_2$  may open up an entirely new line of research for enhancing the efficiency of transition metal dichalcogenides (TMDCs) solar cell.

## COMPUTATIONAL METHODS

Structure searches of monolayer  $\text{MoS}_2$  were carried out with simulation cells of up to 18 atoms using the swarm-intelligence based CALYPSO method<sup>23–27</sup>, which has been benchmarked on various known systems, ranging from elements to binary and ternary compounds.<sup>28–33</sup> The population size was set to 20 and the structure search was terminated after the generation of up to 1,000 structures for each run. Structural optimizations, electronic structures, phonons, and molecular dynamics were performed in the framework of density functional theory (DFT). The generalized gradient approximation (GGA) expressed by PBE functional<sup>34</sup> as implemented in the Vienna Ab initio Simulation Package (VASP)<sup>35</sup> was adopted unless otherwise stated. The electron-ion interaction was described by the projector augmented-wave potentials<sup>36</sup>, with  $4p^6 4d^5 5s^1$  and  $3s^2 3p^4$  configurations treated as the valence electrons of Mo and S, respectively. A kinetic cutoff energy of 500 eV and Monkhorst-Pack  $k$ -mesh sampling of  $12 \times 12 \times 1$  were adopted to ensure well converged total energies ( $\sim 1$  meV/atom). The ionic positions were fully relaxed until the residual force acting on each ion was less than 0.01 eV/Å. Sufficient vacuum was used along  $z$  direction i.e. perpendicular to the 2D sheet, to avoid spurious interaction among the periodic images. The dynamic stability of the predicted new phases was verified from phonon calculation using the direct supercell method as implemented in the PHONOPY code<sup>37,38</sup>. To confirm the thermal stability, ab initio molecular dynamic (AIMD) simulations were carried out with a time step of 1 fs, and the total simulation time was 5 ps. The temperature was controlled at 600 K using the Nosé-Hoover chain thermostat with  $4 \times 4$  supercells that contain 144 atoms. To evaluate the photovoltaic performance, we calculated the theoretical photovoltaic efficiency<sup>39</sup>, which captures the band gap, shape of absorption spectrum and material-dependent non-radiative recombination loss. Note that the standard GGA tends to underestimate the band gaps, thus for  $\text{MoS}_2$  monolayers, we also employed Heyd–Scuseria–Ernzerhof (HSE) hybrid functional<sup>40</sup>, which was proven to be a reliable method for the calculation of electronic structures, to evaluate the band gap values. However, for multilayer

MoS<sub>2</sub> systems, both structural optimizations and band structure computations were carried out by standard PBE functional.

## RESULTS AND DISCUSSION

Through CALYPSO structure searching simulations, the known phases including 1H, 1T, 1T' and 1T'' -MoS<sub>2</sub> have been successfully reproduced, demonstrating the reliability of our methodology in application to MoS<sub>2</sub>. Importantly, our structural searches identified two unknown low-lying phases with *P31m* and *P2/c* symmetries (Fig. 1a and Table S1), denoted as 1T<sub>d</sub>-MoS<sub>2</sub> and 1H'-MoS<sub>2</sub>, respectively. 1T<sub>d</sub> structure can be obtained by distorting the octahedral coordination patterns of Mo atoms in 1T phase, while 1H' phase can be viewed as re-organization of the unit cells of 1H phase (see the red dotted rectangle frame in Fig. 1). 1H' phase is slightly lower in energy than 1T phase (by 38 meV/f.u.). Remarkably, 1T<sub>d</sub> phase is energetically more favorable than the known 1T and 1T' phases by ~300 and 12 meV/f.u. (Fig. 1b), respectively. Moreover, no imaginary phonons have been found in the Brillouin zone of the newly discovered 1T<sub>d</sub> and 1H' phases (Fig. S1), providing direct evidence for their dynamical stability. Furthermore, our AIMD simulations showed that the 1T<sub>d</sub> phase does not suffer obvious structural destruction at 600 K (see Fig. S2). The decent thermal stability also ensures its potential application in photovoltaics. Considering the relative high energy of the 1H' phase and its narrow band gap of 0.34 eV (by HSE functional, Fig. S1c), we will only focus on 1T<sub>d</sub> phase in this work.

Interestingly, 1T<sub>d</sub> phase has a direct band gap of 1.27 eV at the HSE level of theory (Fig. 2a). The dominant contributions to the highest occupied and the lowest unoccupied states are mainly from the *d* orbitals of Mo atoms. Comparing the geometric and electronic structures of 1T<sub>d</sub> and 1T phases, we can find that a subtle change in crystal structure leads to a dramatic difference in the electronic properties: 1T phase, in which the S atoms are in octahedral coordination with Mo atoms, is metallic, whereas 1T<sub>d</sub> phase, in which the S octahedral coordination is only slightly distorted, becomes semiconducting.

The electronic structures of TMDCs strongly depend on the coordination environments of the transition metals and its *d*-electron count, which gives rise to different electronic properties<sup>42</sup>. For MoS<sub>2</sub>, Mo is a divalent ion and has a *d*<sup>2</sup> electron count. In both 1T and 1T<sub>d</sub> phases, the non-bonding *d* states are located within the gap between the bonding ( $\sigma$ ) and antibonding ( $\sigma^*$ ) states (Fig. 2b, Fig. S3).<sup>42</sup> Distorted octahedral coordination of Mo atoms in 1T<sub>d</sub> phase leads to its lower symmetry (*C*<sub>3v</sub>) compared with that of 1T phase (*O*<sub>h</sub>). According to the ligand field theory<sup>43</sup>, there are two degenerated *e<sub>g</sub>* and *t<sub>2g</sub>* orbitals in octahedrally coordinated structures with *O<sub>h</sub>* symmetry: the doubly degenerated *e<sub>g</sub>* orbitals contain *d<sub>z<sup>2</sup></sub>* and *d<sub>x<sup>2</sup>-y<sup>2</sup></sub>* orbitals, and the triply degenerated *t<sub>2g</sub>* orbitals contain *d<sub>xy</sub>*, *d<sub>yz</sub>*, and *d<sub>xz</sub>* orbitals. Since the energy level of *t<sub>2g</sub>* is lower than that of *e<sub>g</sub>*, the occupancy of two *d* electrons of Mo in the three-fold degenerated *t<sub>2g</sub>* orbitals lead to partially filled *d* orbitals, resulting in the metallic character of 1T phase. On the other hand, the *d* orbitals of Mo with *C*<sub>3v</sub> symmetry in 1T<sub>d</sub>

phase splits into one-fold  $a_1$  orbital corresponding to  $d_{z^2}$  orbital and two doubly degenerated  $e$  orbitals corresponding to  $d_{x^2-y^2}$ ,  $d_{xy}$ ,  $d_{xz}$ , and  $d_{yz}$  orbitals. Full occupation of one-fold  $a_1$  orbitals by two Mo electrons defines the semiconducting behavior of  $1T_d$  phase.

We further examined the band structures of  $1T_d$  phase of  $\text{MoS}_2$  with different thickness. At HSE level of theory, both the bilayer and the bulk  $\text{MoS}_2$  keep the direct band-gap nature of the monolayer. The bulk has a gap of 1.36 eV, very close to the monolayer (1.27 eV) and bilayer (1.25 eV). The same trend persists when more multilayers are examined by PBE functional. At the PBE level of theory, the multilayers (with layer numbers of 2, 4, and 6) and the bulk of  $1T_d$  structure remain the direct band-gap nature with their band gap values ranging from 0.68 eV to 0.83 eV (Fig. 2c). These computations indicate that thinning the bulk  $1T_d$  phase of  $\text{MoS}_2$  down to the monolayer does not enhance the quantum confinement of electrons. This is in stark contrast to  $1H$  phase of  $\text{MoS}_2$ , where a transition from direct to indirect band structure occurs as the number of layers increases.<sup>3,44</sup> This difference might result from the much weaker vdW interactions in the multilayer structures of  $1T_d$  phase. As shown in Fig. 2d, the adjacent layers in  $1T_d$  phase only have a coupling energy of 8.67 meV/f.u., much smaller than  $\sim 112$  meV/f.u. in  $1H$  phase, which consists with previous reports<sup>45</sup>. We also chosen the tri-layer  $1T_d$  phase to examine the effect of the different stacking configurations, and found that the total energies and band structures for different stacking patterns are rather similar (Fig. S4). Thus, it is the extremely weak vdW forces between adjacent  $1T_d$  layers that lead to the layer number independent geometric and electronic properties of  $1T_d$  phase.

For a practical solar cell, the theoretical photovoltaic efficiency relies on the thickness of the absorber layer. Thus, we calculated the photovoltaic efficiencies of  $1T_d$   $\text{MoS}_2$  absorber layers as a function of the thickness (Fig. 3) by taking the absorption coefficient and the thickness of absorber layer into consideration.<sup>39</sup> The same computations were performed for  $1H$   $\text{MoS}_2$  layers and GaAs layers for comparison. Evidently, the  $1T_d$   $\text{MoS}_2$  exhibits much higher photovoltaic efficiencies than  $1H$   $\text{MoS}_2$  and GaAs for any given thickness. More importantly,  $1T_d$   $\text{MoS}_2$  layers achieve high efficiencies with very thin absorber layers. For example, 30-nm-thick  $1T_d$   $\text{MoS}_2$ -based cells can have a photovoltaic efficiency up to 33.3%, in stark contrast, only when the thickness of absorbers is about 200 nm can the high efficiency of  $\sim 30.0\%$  in GaAs be achieved.<sup>46-48</sup>

It was recently reported that metastable monolayer TMDCs can be obtained by chemical lithium intercalation<sup>6</sup> and electrostatic-doping<sup>49</sup>. Therefore electron injection may be a practical route to synthesize the newly predicted metastable phases. To evaluate the effects of electron filling on phase stability, we constructed a model system, in which all Mo atoms are replaced by electron richer Tc or Ru atoms. It is found that the  $1T_d$  phases of  $\text{TcS}_2$  and  $\text{RuS}_2$  are energetically more favorable than the corresponding  $1H$  phases (see Fig. 4a), suggesting that the  $1T_d$  phase of  $\text{MoS}_2$  may be obtained by adding one extra electron per unit cell. For comparison, two extra electrons per unit cell<sup>50</sup> are required to obtain the  $1T$  phase of  $\text{MoS}_2$  since only the  $1T$  phase of  $\text{RuS}_2$  is energetically favorable

than the 1H phase. Therefore, the experimental synthesis of  $1T_d$  phase should be more accessible in view of the fewer extra electrons needed. In fact, distorted 1T superstructures have already been observed in experiments<sup>51</sup>; these superstructures may be closely related to our predicted  $1T_d$  phase. In addition, we found that there is a large energy barrier of  $\sim 0.29$  eV/atom (equivalent to  $\sim 3360$  K) between the metastable  $1T_d$  phase and the energetically most favorable 1H phase (see Fig. 4b). Therefore, the  $1T_d$  phase will be kinetically protected once synthesized. The conversion from  $1T_d$  to 1T, and then to 1H would have a lower barrier of  $\sim 0.18$  eV from Fig 4c, indicating other minimum energy reaction paths may exist. Thus, two reaction paths:  $1H \rightarrow 1T$  and  $1T \rightarrow 1T_d$  have been calculated. As illustrated in Figure S5, the energy barrier from 1H to 1T is 0.08 eV/atom and no energy barrier is found from 1T to  $1T_d$ . If going from right to left, indeed, there is an energy barrier of 0.18 eV/atom (equivalent to  $\sim 2089$  K) from  $1T_d$  to 1H.

Our phonon dispersion computations showed that the free-standing 1T phase has two imaginary phonon modes at A ( $-1/3 \ 1/3 \ 0$ ) and M point ( $0 \ 1/2 \ 0$ ) (see the inset of Fig. 4c), signifying its decisive role in characterizing phase transitions. To confirm this, we produced the distorted structures by freezing the amplitudes of the atomic displacements along the normal coordinates of the softening phonon, then calculated the total energies for a series of atomic displacements along the vibrations corresponding to the A and M points while maintaining the rest of the structural parameters at the referenced structure values (see Fig. 4c). As expected, the  $1T_d$  and  $1T'$  phases were identified during our structural optimizations. Since the  $1T_d$  structure is energetically more favorable than  $1T'$ , there is a higher possibility that the freestanding 1T phase eventually transforms to the  $1T_d$  phase, which was confirmed by our AIMD simulations: the freestanding 1T-MoS<sub>2</sub> phase would undergo a spontaneous distortion, leading to the  $1T_d$  phase at low temperature (300 K); however,  $1T_d$  phase can only transform into 1T phase at 1000 K (Fig. S6). These findings demonstrate a feasible approach for active control of the experimental realization of  $1T_d$  phase from experimentally synthesized 1T phase. In addition, the weak vdW interactions in the multilayer structures of  $1T_d$  phase implies that freestanding monolayer can be also easily produced from bulk  $1T_d$  phase by exfoliation. To assist the future experimental characterization, we simulated the occupied state STM images at a bias of -0.5 V for the 1H, 1T,  $1T_d$  and  $1T'$  MoS<sub>2</sub> (Fig. S7). Note that our simulated STM images of 1H phase<sup>52</sup> and  $1T'$  phase<sup>18</sup> well agree with experiments. Meanwhile, we also calculated the atomic vibrations for each mode of  $1T_d$  and 1H phase (Table S2). The good agreement between two computed and experimentally measured Raman peaks, labeled as  $E_{2g}^1$  and  $A_{1g}$ , for 1H MoS<sub>2</sub> monolayer,<sup>53</sup> supports the validity and accuracy of our computational procedure.

It is known that the first synthesized metastable  $1T'$ -TMDCs phase is MoTe<sub>2</sub> instead of MoS<sub>2</sub>. It is of significant importance to study the stabilities and electronic properties of other five  $1T_d$ -TMDCs phases: MoSe<sub>2</sub>, MoTe<sub>2</sub>, WS<sub>2</sub>, WSe<sub>2</sub> and WTe<sub>2</sub>. By comparing the energies of the  $1T_d$ -, 1T-,  $1T'$ - and 1H-phases (Fig. S8), we found that all  $1T_d$  phases are energetically more favorable than the 1T



phases. It is seen from Fig. S8 that all the  $1T_d$ - TMDCs are semiconductors with direct band gaps of which the values range from 1.10 to 1.34 eV at the HSE06 level (Fig. S8). The suitable band gaps endow  $1T_d$  phase with potential applications in solar cells.

## Conclusion

In summary, a new semiconducting phase ( $1T_d$ ) of monolayer  $\text{MoS}_2$  with an optimal, direct optical band gap of 1.27 eV is discovered by the global optimization swarm intelligence algorithm. Thermodynamically this newly predicted monolayer is slightly more favorable than the recently synthesized  $1T'$  phase. Due to the rather weak interlayer interactions, the geometric and electronic properties of  $1T_d$  phase is nearly independent of layer number, especially its direct band gap nature persists in multilayers, and the band gap values can be slightly tuned by controlling the layer number. The photovoltaic efficiency of the  $1T_d$  phase reaches  $\sim 33.3\%$ , which is close to the Shockley–Queisser limit, at only  $\sim 0.3 \mu\text{m}$  thickness. Our computations also suggest that it is highly promising to synthesize the  $1T_d$  phase by electron injection, and it is also feasible to convert the experimentally synthesized  $1T$  phase to  $1T_d$  phase by proper annealing. Once synthesized, the superior photovoltaic property of the  $1T_d$  phase may open a door to further exploring new high-performance TMD-based solar cells.

## Supporting Information

Crystallographic Data of  $1T_d$  and  $1H'$  phases; the Raman peaks of  $1T_d$  and  $1H$  phase; phonon dispersions and the band structures calculated from HSE06 functional of  $1H'$  phase; the AIMD simulations of  $1T_d$  phase at 600 K; further analysis on the orbital levels of  $1T_d$ - $\text{MoS}_2$ ; the optimized structures and band gaps of tri-layer  $1T_d$ - $\text{MoS}_2$  with three stacking configurations; different images on minimum energy path from  $1H$  to  $1T$  and  $1T$  to  $1T_d$  phases; AIMD simulations of the temperature-induced phase transition between  $1T_d$  phase and  $1T$  phase; the simulated occupied state STM images for  $1H$ ,  $1T_d$ ,  $1T'$  and  $1T$  phases; the total energies and band structures of the other five  $\text{MX}_2$  monolayers in  $1T_d$  phase; computational method for spectroscopic limited maximum efficiency (SLME).

## AUTHOR INFORMATION

### Corresponding Authors

yuechen@hku.hk

wyc@calypso.cn

mym@calypso.cn

### Notes

The authors declare no competing financial interest.

## ACKNOWLEDGEMENTS

The authors acknowledge funding support from the National Natural Science Foundation of China

under Grants No. 11774127, No. 11534003 and No. 11764043; the National Key Research and Development Program of China under Grant No. 2016YFB0201200, No. 2016YFB0201201, and No. 2017YFB0701503; the 2012 Changjiang Scholars Program of China supported by Program for JLU Science and Technology Innovative Research Team (JLUSTIRT); the Science Challenge Project, No. TZ2016001, the Research Grants Council of Hong Kong under Grant No. 27202516 and the NSF-CREST Center for Innovation, Research and Education in Environmental Nanotechnology (CIRE2N) (Grant Number HRD-1736093) and NASA (Grant 17-EPSCoRProp-0032). Part of the calculation was performed in the high performance computing center of Jilin University and at Tianhe2-JK in the Beijing Computational Science Research Center.

## References

1. Wang, Q. H., Kalantar-Zadeh, K., Kis, A., Coleman, J. N. & Strano, M. S. Electronics and optoelectronics of two-dimensional transition metal dichalcogenides. *Nat. Nanotechnol.* **7**, 699–712 (2012).
2. Mak, K. F. & Shan, J. Photonics and optoelectronics of 2D semiconductor transition metal dichalcogenides. *Nat. Photonics* **10**, 216–226 (2016).
3. Mak, K. F., Lee, C., Hone, J., Shan, J. & Heinz, T. F. Atomically thin MoS<sub>2</sub>: A new direct-gap semiconductor. *Phys. Rev. Lett.* **105**, 2–5 (2010).
4. Wu, Z. *et al.* MoS<sub>2</sub> nanosheets: A designed structure with high active site density for the hydrogen evolution reaction. *ACS Catal.* **3**, 2101–2107 (2013).
5. Tye, C. T. & Smith, K. J. Catalytic activity of exfoliated MoS<sub>2</sub> in hydrodesulfurization, hydrodenitrogenation and hydrogenation reactions. *Top. Catal.* **37**, 129–135 (2006).
6. Chang, K. *et al.* Targeted Synthesis of 2H- and 1T-Phase MoS<sub>2</sub> Monolayers for Catalytic Hydrogen Evolution. *Adv. Mater.* **28**, 10033–10041 (2016).
7. Tang, Q. & Jiang, D. E. Mechanism of Hydrogen Evolution Reaction on 1T-MoS<sub>2</sub> from First Principles. *Acs Catal.* **6**, 4953–4961 (2016).
8. Zong, X. *et al.* Enhancement of photocatalytic H<sub>2</sub> evolution on CdS by loading MoS<sub>2</sub> as cocatalyst under visible light irradiation. *J. Am. Chem. Soc.* **130**, 7176–7177 (2008).
9. Voiry, D. *et al.* Conducting MoS<sub>2</sub> nanosheets as catalysts for hydrogen evolution reaction. *Nano Lett.* **13**, 6222–6227 (2013).
10. Ganatra, R. & Zhang, Q. Few-layer MoS<sub>2</sub>: A promising layered semiconductor. *ACS Nano* **8**, 4074–4099 (2014).
11. Zibouche, N., Philipsen, P., Kuc, A. & Heine, T. Transition-metal dichalcogenide bilayers: Switching materials for spintronic and valleytronic applications. *Phys. Rev. B* **90**, 125440 (2014).
12. Singh, E., Kim, K. S., Yeom, G. Y. & Nalwa, H. S. Atomically thin-layered molybdenum disulfide (MoS<sub>2</sub>) for bulk-heterojunction solar cells. *ACS Appl. Mater. Interfaces* **9**, 3223–3245 (2017).
13. Xu, Z. *et al.* Monolayer MoS<sub>2</sub>/GaAs heterostructure self-driven photodetector with extremely high detectivity. *Nano Energy* **23**, 89–96 (2016).
14. Tsai, M.-L. *et al.* Monolayer MoS<sub>2</sub> Heterojunction Solar Cells. *ACS Nano* **8**, 8317–8322 (2014).
15. Lin, S. *et al.* Interface designed MoS<sub>2</sub>/GaAs heterostructure solar cell with sandwich stacked hexagonal boron nitride. *Sci. Rep.* **5**, 15103 (2015).
16. Pradhan, S. K., Xiao, B. & Pradhan, A. K. Enhanced photo-response in p-Si/MoS<sub>2</sub> heterojunction-based solar cells. *Sol. Energy Mater. Sol. Cells* **144**, 117–127 (2016).

17. Rao, C. N. R. & Maitra, U. Inorganic Graphene Analogs. *Annu. Rev. Mater. Res.* **45**, 29–62 (2015).
18. Yu, Y. *et al.* High phase-purity 1T'-MoS<sub>2</sub>- and 1T'-MoSe<sub>2</sub>-layered crystals. *Nat. Chem.* **10**, 638 (2018).
19. Qian, X., Liu, J., Fu, L. & Li, J. Quantum spin Hall effect in two-dimensional transition metal dichalcogenides. *Science* **346**, 1344–1347 (2014).
20. Ma, F. *et al.* Predicting a new phase (T'') of two-dimensional transition metal di-chalcogenides and strain-controlled topological phase transition. *Nanoscale* **8**, 4969–4975 (2016).
21. Bernardi, M., Palummo, M. & Grossman, J. C. Extraordinary sunlight absorption and one nanometer thick photovoltaics using two-dimensional monolayer materials. *Nano Lett.* **13**, 3664–3670 (2013).
22. Britnell, L. *et al.* Strong Light-Matter Interactions in Heterostructures of Atomically Thin Films. *Science* **340**, 1311–1314 (2013).
23. Wang, Y. & Ma, Y. Perspective: Crystal structure prediction at high pressures. *J. Chem. Phys.* **140**, 040901 (2014).
24. Wang, Y., Lv, J., Zhu, L. & Ma, Y. Crystal structure prediction via particle-swarm optimization. *Phys. Rev. B* **82**, 094116 (2010).
25. Wang, Y., Lv, J., Zhu, L. & Ma, Y. CALYPSO: A method for crystal structure prediction. *Comput. Phys. Commun.* **183**, 2063–2070 (2012).
26. Wang, Y. *et al.* Materials discovery via CALYPSO methodology. *J. Phys. Condens. Matter* **27**, 203203 (2015).
27. Wang, Y. *et al.* An effective structure prediction method for layered materials based on 2D particle swarm optimization algorithm. *J. Chem. Phys.* **137**, 224108 (2012).
28. Zhu, L. *et al.* Substitutional Alloy of Bi and Te at High Pressure. *Phys. Rev. Lett.* **106**, 145501 (2011).
29. Zhu, L., Liu, H., Pickard, C. J., Zou, G. & Ma, Y. Reactions of xenon with iron and nickel are predicted in the Earth's inner core. *Nat. Chem.* **6**, 644 (2014).
30. Xu, M. *et al.* Anatase (101)-like Structural Model Revealed for Metastable Rutile TiO<sub>2</sub>(011) Surface. *ACS Appl. Mater. Interfaces* **9**, 7891–7896 (2017).
31. Lv, J., Wang, Y., Zhu, L. & Ma, Y. Predicted Novel High-Pressure Phases of Lithium. *Phys. Rev. Lett.* **106**, 015503 (2011).
32. Li, Y., Hao, J., Liu, H., Li, Y. & Ma, Y. The metallization and superconductivity of dense hydrogen sulfide. *J. Chem. Phys.* **140**, 174712 (2014).
33. Wang, H., Tse, J. S., Tanaka, K., Iitaka, T. & Ma, Y. Superconductive sodalite-like clathrate calcium hydride at high pressures. *Proc. Natl. Acad. Sci.* **109**, 6463–6466 (2012).
34. Perdew, J. P., Burke, K. & Ernzerhof, M. Generalized Gradient Approximation Made Simple.

- Phys. Rev. Lett.* **77**, 3865–3868 (1996).
35. Kresse, G. & Furthmüller, J. Efficient iterative schemes for ab initio total-energy calculations using a plane-wave basis set. *Phys. Rev. B* **54**, 11169–11186 (1996).
  36. Kresse, G. & Joubert, D. From ultrasoft pseudopotentials to the projector augmented-wave method. *Phys. Rev. B* **59**, 1758–1775 (1999).
  37. Parlinski, K., Li, Z. & Kawazoe, Y. First-Principles Determination of the Soft Mode in Cubic  $\text{ZrO}_2$ . *Phys. Rev. Lett.* **78**, 4063–4066 (1997).
  38. Togo, A., Oba, F. & Tanaka, I. First-principles calculations of the ferroelastic transition between rutile-type and  $\text{CaCl}_2$ -type  $\text{SiO}_2$  at high pressures. *Phys. Rev. B* **78**, 134106 (2008).
  39. Yu, L. & Zunger, A. Identification of potential photovoltaic absorbers based on first-principles spectroscopic screening of materials. *Phys. Rev. Lett.* **108**, 68701 (2012).
  40. Heyd, J., Scuseria, G. E. & Ernzerhof, M. Hybrid functionals based on a screened Coulomb potential. *J. Chem. Phys.* **118**, 8207–8215 (2003).
  41. Walle, H. P. and C. G. Van de. First-principles study of van der Waals interactions in  $\text{MoS}_2$  and  $\text{MoO}_3$ . *J. Phys. Condens. Matter* **26**, 305502 (2014).
  42. Chhowalla, M. *et al.* The chemistry of two-dimensional layered transition metal dichalcogenide nanosheets. *Nat. Chem.* **5**, 263–275 (2013).
  43. Griffith, J. S. & Orgel, L. E. Ligand-field theory. *Quart. Rev. Chem. Soc.* **11**, 381–393 (1957).
  44. Kuc, A., Zibouche, N. & Heine, T. Influence of quantum confinement on the electronic structure of the transition metal sulfide  $\text{TS}_2$ . *Phys. Rev. B* **83**, 245213 (2011).
  45. Tongay, S. *et al.* Monolayer behaviour in bulk  $\text{ReS}_2$  due to electronic and vibrational decoupling. *Nat. Commun.* **5**, 1–6 (2014).
  46. Green, M. A., Emery, K., Hishikawa, Y. & Warta, W. Solar cell efficiency tables (version 37). *Prog. Photovoltaics Res. Appl.* **19**, 84–92 (2011).
  47. Shah, A. Photovoltaic Technology: The Case for Thin-Film Solar Cells. *Science*, **285**, 692–698 (1999).
  48. Takamoto T, Ikeda E, Kurita H, et al. Two-terminal monolithic  $\text{In}_{0.5}\text{Ga}_{0.5}\text{P}/\text{GaAs}$  tandem solar cells with a high conversion efficiency of over 30%. *Jpn. J. Appl. Phys.* **36**, 6215 (1997)
  49. Wang, Y. *et al.* Structural phase transition in monolayer  $\text{MoTe}_2$  driven by electrostatic doping. *Nature* **550**, 487–491 (2017).
  50. Gao, G. *et al.* Charge Mediated Semiconducting-to-Metallic Phase Transition in Molybdenum Disulfide Monolayer and Hydrogen Evolution Reaction in New 1T' Phase. *J. Phys. Chem. C* **119**, 13124–13128 (2015).
  51. Heising, J. & Kanatzidis, M. G. Exfoliated and Restacked  $\text{MoS}_2$  and  $\text{WS}_2$ : Ionic or Neutral Species? Encapsulation and Ordering of Hard Electropositive Cations. *J. Am. Chem. Soc.* **121**, 11720–11732 (1999).

52. Hong, J. *et al.* Direct Imaging of Kinetic Pathways of Atomic Diffusion in Monolayer Molybdenum Disulfide. *Nano Lett.* **17**, 3383–3390 (2017).
53. Hong, L. *et al.* From bulk to monolayer MoS<sub>2</sub>: evolution of Raman scattering. *Adv. Funct. Mater.* **22**(7), 1385-1390 (2012)

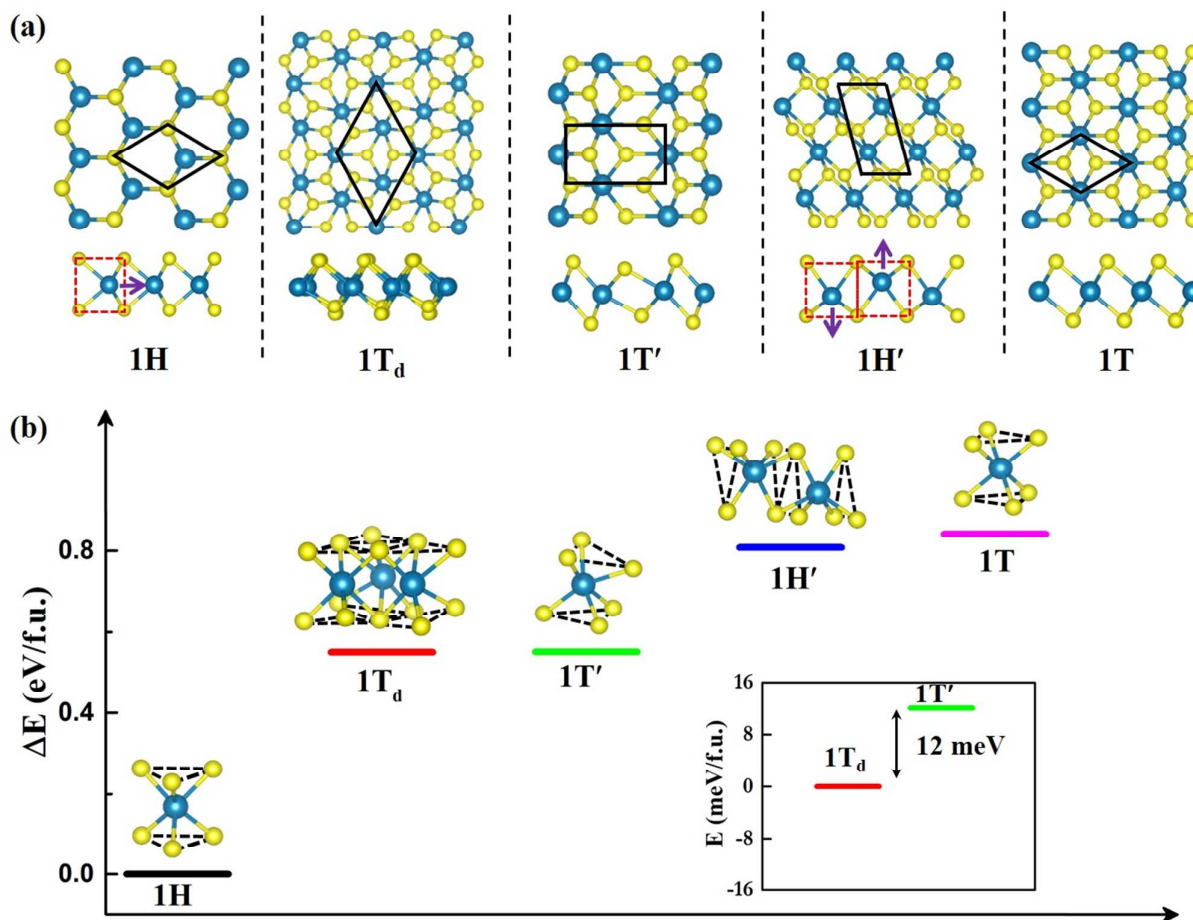


Figure 1. (a) Atomic structures of monolayer MoS<sub>2</sub> in 1H, 1T<sub>d</sub>, 1T', 1H', and 1T phases. The unit cells are indicated by black solid lines. (b) The calculated total energies (per MoS<sub>2</sub> formula unit relative to 1H phase) and the basic building blocks.

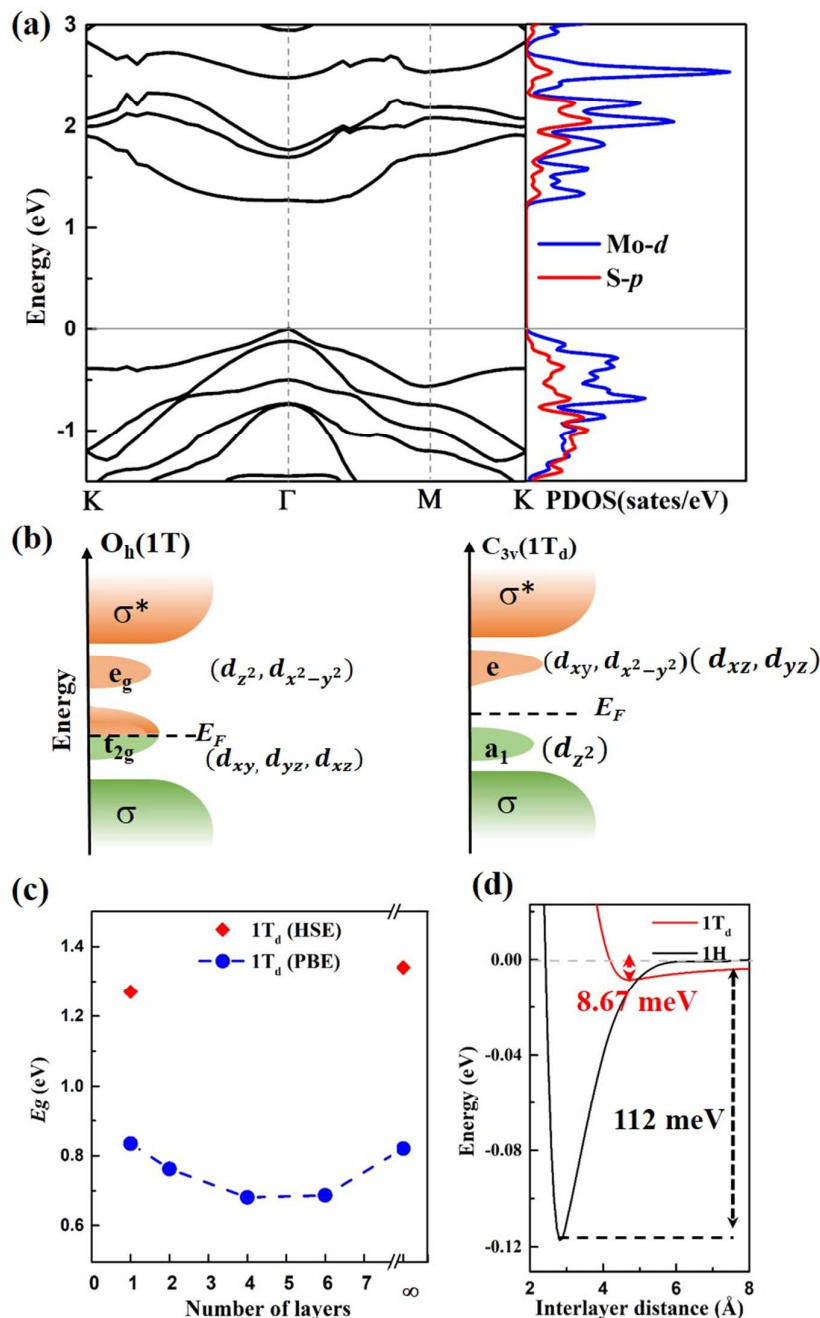
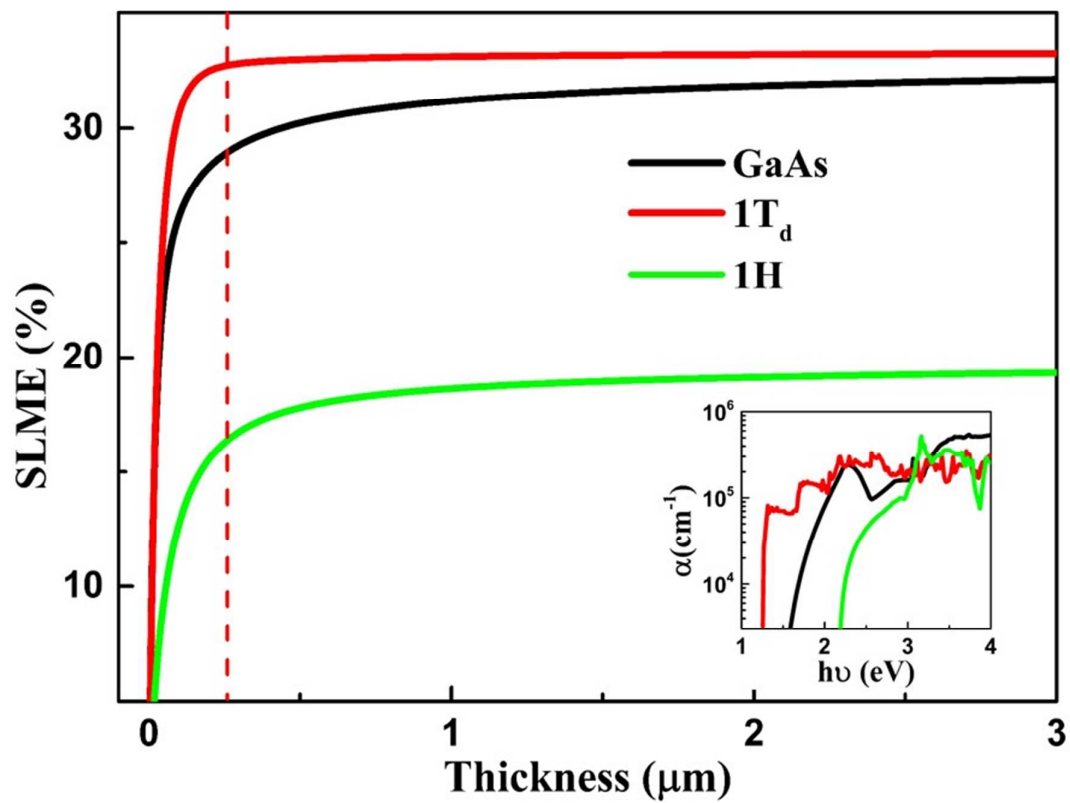


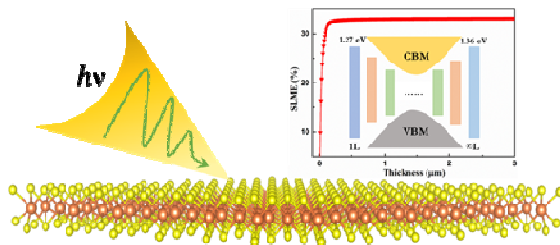
Figure 2. (a) Band structure and density of states of 1T<sub>d</sub>-MoS<sub>2</sub> phase at HSE level. (b) Schematic illustration showing the progressive filling of d orbitals that are located within the band gap of bonding ( $\sigma$ ) and anti-bonding states ( $\sigma^*$ ) in MoS<sub>2</sub>. (c) Calculated band gap ( $E_g$ ) as a function of number of layers. (d) The coupling energy of the system as a function of interlayer separation. The different  $d$ -orbital splitting in crystal structures with octahedral (1T) and distorted octahedral (1T<sub>d</sub>) geometries. O<sub>h</sub> and C<sub>3v</sub> refer to the point groups associated with the 1T and 1T<sub>d</sub> phases, respectively. The filled and unfilled states are shaded with green and light orange, respectively.





**Figure 3.** SLME as a function of slab thickness for 1T<sub>d</sub> phase compared with 1H-MoS<sub>2</sub> and GaAs. The inset shows their adsorption spectra.





We predict a novel 1T<sub>d</sub>-MoS<sub>2</sub> with a direct band gap of 1.27 eV which reaches high photovoltaic efficiency of ~33.3%.